Journal of Structural Geology, Vol. 9, No. 8, pp. 1039 to 1046, 1987
Printed in Great Britain

0191-8141/87 $03.00 + 0.00

Distributions of cumulative displacement and seismic slip on a single normal fault surface

J. J. WALSH and J. WATTERSON

Department of Geological Sciences, University of Liverpool, P.O. Box 147, Liverpool L69 3BX, U.K.

(*Received* 21 *October* 1986; *accepted in revised form* 1 *May* 1987)

Abstract—Displacement profiles (normalized displacement vs normalized distance from the point of maximum displacement) have been plotted for 34 horizontal radii from 25 normal faults with maximum displacements ranging from 1.0 to 37.5 m. The composite displacement profile for these faults, when corrected for systematic inaccuracies of the data, is significantly different from the theoretical slip profile for a single seismic slip event. The integration of slip displacement profiles of many slip events on a growing fault shows that a steady-state displacement profile will be established. This theoretical displacement profile is similar to the composite profile derived from the fault data. Analysis of displacement data from 488 fault traces, which do not necessarily pass through the point of maximum displacement of their respective faults, shows that although displacement measurements are strongly influenced by ductile drag the theoretical distribution can still be identified in the data. Although the slip distribution on a fault during a single slip event, or during a period of stable sliding, is not simply related to the distribution of cumulative displacement on the fault, a knowledge of both characteristics places firm constraints on fault growth models.

INTRODUCTION

AN IDEAL single fault is one which does not intersect its contemporary surface and on which displacement is not transferred onto a splay or other structure. Faults which bound major crustal blocks and gravity-driven growth faults are excluded from the following discussion. Fault surfaces are usually non-planar and although this poses some geometrical and mechanical problems concerning variable displacement, they do not significantly affect the following analysis and are not discussed further. Displacement on a fault refers to the total cumulative displacement resulting from a number of discrete slip events or from an extended period of stable sliding: data are available for inactive faults where they have been intersected by mining operations or where high-resolution seismic reflection data are available. The displacement on a single fault surface ideally varies from a maximum at the centre to zero at the tip-line which forms a closed loop analogous to a dislocation loop in a crystal. The tip-line loop has been shown, in ideal cases, to be elliptical for simple faults intersected by coal-mining operations (Rippon 1985) and similar elliptical loops characterize faults reconstructed from offshore seismic reflection data (Barnett *et al.* 1987). In both cases the ellipses have axial ratios of between 2:1 and 3:1 with the minor axis of the ellipse parallel to the displacement direction on normal faults, and the major axis parallel to the bedding of near horizontal sedimentary rocks. It is not yet known whether the slip direction determines the orientation of the tip-line ellipse, or whether both the orientation and the axial ratio of the ellipse are determined by the orientation and degree of mechanical anisotropy of the faulted sedimentary succession.

Within the tip-line loop, contours of displacement plot as a series of concentric ellipses centred on the point of maximum displacement: a fault does not therefore have a single displacement vector, but has vectors of varying magnitude systematically distributed over the fault surface (Barnett *et al.* 1987). This paper is concerned with the differences between the systematic distribution of displacement over a fault surface, and the systematic distribution of slip on a fault surface during a single earthquake event, and with how these differences can be reconciled. Radial distributions of displacement and of slip are discussed in terms of simple idealized models; these can be shown to be realistic simplifications of the real phenomena.

Measurements of fault displacements recorded on mine plans, and those derived from seam contours, are for vertical displacement or throw. In the following all reference to, and plotting of, displacement data from coalfield faults is in terms of vertical displacement unless indicated otherwise.

DISPLACEMENT DISTRIBUTION ON FAULT SURFACES

There is a continuum between structures in which shear displacement is accommodated entirely on discontinuity surfaces, as in many faults, and those in which no discontinuity is developed, as in ductile shear zones. This account is concerned primarily with those in which the shear displacement is largely or entirely accommodated on discontinuity surfaces, but the general principles are applicable to all combinations of discontinuous and continuous displacements.

Data have been derived from either complete or partial displacement contour diagrams of normal faults occurring in the English East Pennine coalfield (Table

Table 1. Normalized displacement values along 34 horizontal fault radii of 25 contoured coalfield normal faults. Normalized distance along fault radius increases towards the tip-line. Measured values of radius and maximum displacement are also shown

Fault No.	Normalized distance (m) 0.10	0.20	0.30	0.40	0.50	0.60	0.70	0.80	0.90	Maximum displacement (m)	Width (m)
1	0.94	0.83	0.68	0.53	0.44	0.41	0.35	0.21	0.10	1.50	310
2	0.99	0.99	0.96	0.66	0.36	0.23	0.16	0.09	0.04	4.00	600
3	0.91	0.82	0.74	0.68	0.61	0.55	0.42	0.19	0.08	4.00	1300
4	0.99	0.97	0.91	0.76	0.35	0.26	0.17	0.11	0.05	3.20	590
5	0.94	0.88	0.79	0.70	0.59	0.48	0.36	0.24	0.12	3.20	700
6	0.92	0.78	0.68	0.64	0.72	0.82	0.64	0.40	0.18	1.50	275
7	0.94	0.84	0.68	0.49	0.39	0.31	0.23	0.15	0.07	1.50	260
8	0.89	0.85	0.82	0.79	0.45	0.23	0.21	0.15	0.05	19.10	1950
9	0.94	0.90	0.85	0.79	0.70	0.58	0.42	0.23	0.11	20.00	600
10	0.97	0.93	0.89	0.85	0.84	0.81	0.68	0.19	0.04	37.50	1235
11	0.98	0.86	0.72	0.61	0.52	0.34	0.23	0.11	0.06	21.30	790
12	0.97	0.94	0.69	0.52	0.39	0.29	0.19	0.12	0.05	15.95	990
13	0.95	0.90	0.85	0.79	0.72	0.64	0.55	0.41	0.19	3.50	1430
14	0.99	0.96	0.89	0.70	0.66	0.64	0.55	0.25	0.12	1.25	275
15	0.89	0.78	0.67	0.58	0.55	0.53	0.48	0.39	0.12	1.25	320
16	0.94	0.87	0.77	0.56	0.36	0.25	0.17	0.11	0.05	2.00	260
17	0.96	0.92	0.86	0.78	0.59	0.33	0.21	0.14	0.07	2.00	170
18	0.93	0.85	0.77	0.67	0.57	0.47	0.35	0.23	0.11	1.00	440
19	0.95	0.89	0.82	0.75	0.65	0.55	0.45	0.33	0.20	1.00	350
20	0.97	0.93	0.88	0.80	0.68	0.54	0.40	0.24	0.11	2.00	540
21	0.96	0.91	0.85	0.72	0.57	0.43	0.34	0.23	0.12	2.70	250
22	0.97	0.89	0.73	0.65	0.57	0.47	0.33	0.17	0.07	9.50	620
23	0.77	0.60	0.46	0.38	0.32	0.24	0.13	0.05	0.01	9.90	600
24	0.95	0.88	0.68	0.62	0.45	0.32	0.21	0.14	0.07	9.20	400
25	0.87	0.74	0.59	0.40	0.29	0.26	0.23	0.16	0.08	9.00	380
26	0.97	0.93	0.89	0.82	0.74	0.68	0.54	0.27	0.10	8.10	990
27	0.85	0.69	0.53	0.38	0.24	0.12	0.06	0.03	0.01	7.60	380
28	0.70	0.51	0.35	0.26	0.21	0.17	0.12	0.06	0.01	7.60	425
29	0.82	0.68	0.60	0.55	0.45	0.32	0.21	0.12	0.05	9.10	400
30	0.84	0.66	0.49	0.30	0.18	0.11	0.07	0.04	0.01	7.10	610
31	0.99	0.98	0.96	0.93	0.88	0.77	0.47	0.33	0.06	18.20	710
32	0.98	0.97	0.95	0.93	0.86	0.55	0.42	0.28	0.07	18.20	960
33	0.67	0.58	0.51	0.45	0.38	0.27	0.12	0.05	0.02	17.20	2270
34	0.92	0.55	0.47	0.31	0.26	0.23	0.19	0.12	0.06	17.20	1710

1). More information is available on displacement distributions along the horizontal major axes of elliptical fault loops than along the minor axes, but there is sufficient information on displacement changes along minor axes to demonstrate a similar distribution. Data are available for the displacement distributions along 34 fault radii from 25 individual faults on which the maximum displacement ranges from 1.0 to 37.5 m. A normalized displacement profile (displacement vs distance from fault centre) has been plotted for each horizontal radius. These have been constructed from displacement contour diagrams (Rippon 1985) which have in turn been constructed from measured values of vertical throw on the same fault encountered in three or more seams, or from throws calculated from seam contours. The density of the archive data is variable and there are no means of checking the recorded measurements. The horizontal major axis of a fault may not coincide with a coal seam and in most cases the position and value of the maximum throw must be interpolated.

Faults are terminated on mine plans where they cease to be of mining significance and the minimum throw values recorded are usually 6 in. or 10 cm in more recent times. It is likely therefore, that mine plans systematically show faults to be shorter than they are and that the underestimate is likely to be unrelated to fault size. Accordingly, 50 m, the approximate radius of a 10 cm fault (Watterson 1986, Barnett *et al.* 1987), has been added to each of the fault radii by displacing the zero contour, extending the radius by 29% in the case of the smallest fault and by 2.2% in the case of the largest. There is some variation in the way in which drag displacement, where it occurs, has been treated by individual mine surveyors. In some cases the drag displacement is included in the displacement measurement, whereas it appears not to have been included in other cases. In the latter case, variation along a fault in the proportion of displacement accommodated by drag will influence the contour pattern and the displacement profile derived from it. While these shortcomings of the data do not permit much significance being attached to differences between individual profiles, a composite profile (Fig. 1) is regarded as representative of the displacement variation: data for the individual profiles are given in Table 1. This normalized profile has been constructed from the 34 individual profiles by measuring displacement on each profile at regular intervals along the normalized radii and using the median value of the 34 measurements to plot the composite curve. It is recognized that this procedure may obscure genuine differences which may exist within the sample but until more data are available this conservative approach is preferred.

Comparable fault data are given by Muraoka &

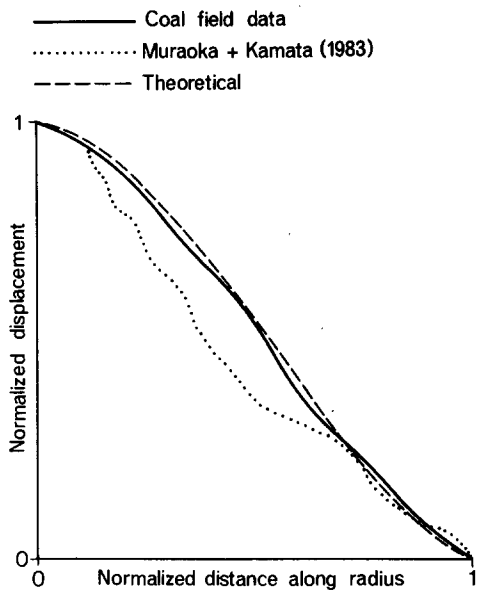

Fig. 1. Normalized displacement profiles along horizontal fault radii for the composite of the contoured coalfield normal faults, for the theoretical fault growth model, and along the vertical radius for composite of the normal faults in Japan (Muraoka & Kamata 1983).

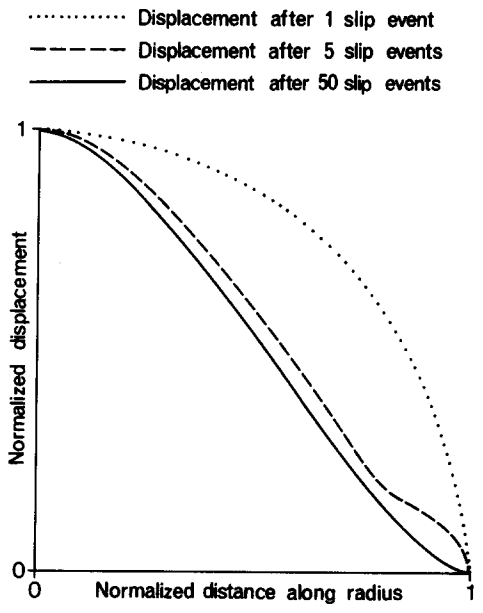

Fig. 2. Normalized slip/displacement profiles after 1, 5 and 50 slip events on a growing fault. Solid curve (50 slip events) represents the steady state and is the theoretical profile plotted in Figs. 1, 5 and 6.

Kamata (1983) whose composite displacement profile (Fig. 1), is derived from data on displacement variation along a radius parallel to the length of a fault, i.e. parallel to the slip direction.

The displacement distribution of the composite profile is quite distinct from that expected for the slip of a fault during a single earthquake event, which is described below.

SLIP DISTRIBUTION ON ACTIVE FAULTS

Slip refers to the movement on a fault either during an earthquake slip event or during an interval of some tens of years of stable sliding. On this time-scale, the distributions of slip is a function of the elastic properties of the rock and can be analysed in terms of an elastic dislocation. The standard solution is that given by Eshelby (1957) for an elastic dislocation remote from a free surface and the predicted distribution of slip over the slip surface is shown in Fig. 2. The main characteristic is that the slip gradient (change in displacement/radial distance) is low over most of the slip surface and that the reduction to zero slip is accommodated mostly within a narrow zone adjacent to the tip-line loop of the slip surface. The slip profile is elliptical and normalizes to a circular profile which is quite distinct from the data profile shown in Fig. 1.

Determinations of slip distribution on actual fault surfaces during seismic slip events, based on either seismic or geodetic data, are not sufficiently accurate to discriminate between alternative profiles but the elliptical distribution shown in Fig. 2 has been reproduced experimentally (Archuleta & Brune 1975).

RELATIONSHIP BETWEEN SLIP AND DISPLACEMENT

Consideration of the differences between the distributions of short-term slip and long-term displacement must take account of the different relationship between displacement and fault dimensions on the one hand, and slip and fault dimensions on the other. Whereas maximum displacement increases approximately with the square of the fault radius (Watterson 1986), maximum slip increases linearly with fault radius (Kanamori & Anderson 1975, Scholz 1982). So long as a fault is active the total displacement will increase with time and the fault radius will also increase. As the maximum slip in each slip event is proportional to the fault radius, the slip must also increase with each successive slip event. Similar considerations mean that in faults which move aseismically by stable sliding, the rate of sliding must also increase with the increase in fault radius and with time. Details of the growth model are not crucial for the present purposes, but it is argued elsewhere (Watterson 1986, Walsh & Watterson 1987) that the maximum slip in successive slip events increases by a constant amount, with the values of maximum slip in a succession of slip events forming an arithmetic series. Both the maximum slip and the fault radius will increase throughout the active life of a fault. Although the pattern of slip distribution over a fault surface is the same for every slip event, the incremental displacements at a point on the fault surface are not identical in successive slip events because the dimensions of the fault surface increase with each slip event. This is shown diagrammatically in Fig. 3. Following the first slip increment the displacement profile will gradually diverge from that of the slip profiles. The displacement profile

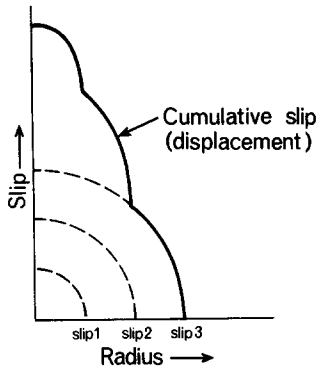

Fig. 3. Diagrammatic illustration of slip in three successive events on a growing fault and the resulting cumulative displacement.

reaches a steady state after a relatively small number of slip increments, or after a correspondingly small amount of slip by stable sliding (Fig. 2).

The steady state distribution found by iteration is illustrated in Fig. 2, and is achieved after 50 slip events with the particular growth model used, in which maximum slip in each successive event is incremented by 0.05 cm.

The expression (see Appendix for derivation) for the steady state normalized profile characteristic of an arithmetic growth model is:

$$d = 2(((1 + r)/2)^2 - r^2)^{1/2}(1 - r),$$

where d is the normalized displacement at a point on a radius of the fault ellipse, and r is the normalized radial distance from centre of the fault.

For this expression, displacement variations along chords on a circular or elliptical fault have normalized profiles which are different from those along the radii of the fault: the differences are not great even in extreme cases of chords remote from the centre (Fig. 4).

A good approximation to the theoretical profile is given by:

$$d = (1 - r^2)^2.$$

For this expression, chords have normalized displacement profiles identical with those along fault radii.

The theoretical profile is closely matched by the composite profile for coalfield faults (Fig. 1): the mismatch between these profiles and that given by Muraoka & Kamata (1983) could be due to the latter being derived from measurements along the lengths of faults rather than along widths. Width data on a normal fault in flat-lying sedimentary rocks are obtained from within a single lithology whereas the fault length may span several different lithologies: displacement gradients vary according to material properties of the rocks (Walsh & Watterson 1987) and this may complicate displacement profiles spanning different lithologies, especially where the fault dimensions are only a few times greater than the thickness of the layering. Lithological variation may also exacerbate complications arising from post-faulting compaction when the faults occur in only partly consolidated sediments, as is the case with those described by Muraoka & Kamata (1983).

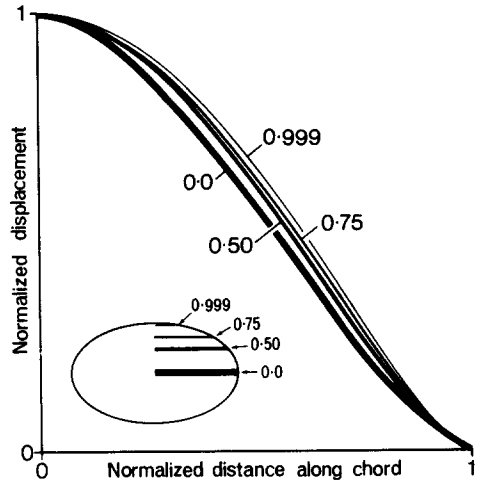

Fig. 4. Theoretical displacement profile along radius (0.0) and along chords at 0.5, 0.75 and 0.999 radial distance from the centre of fault, as shown in inset.

The conclusion drawn is that the slip distribution on a fault during a single earthquake event is not simply related to the distribution of cumulative displacement on that or similar faults, but that the two are related by a simple growth model and that a knowledge of one places firm contraints on the other. Alternatively, a knowledge of both single slip and cumulative displacement profiles places firm constraints on growth model parameters.

FAULT TRACE ANALYSIS

For most faults, whether examined on mine plans, structural contour maps, seismic sections or in the field, displacement data are available only on single fault traces (i.e. the line of intersection with a seam, reflector, seismic line or outcrop surface). The trace therefore represents a chord of the fault ellipse at an unknown distance from the fault centre, although the orientation relative to the displacement vector is often known. It was shown earlier (Fig. 4) that theoretical normalized profiles along chords are not very different from those along a radius of a fault ellipse. Data have been assembled to investigate the possible uses of chord profiles.

Fault traces recorded on mine plans have been selected according to the following criteria: (i) the fault trace terminates in worked ground; (ii) a maximum displacement is identifiable on the trace, either because it is flanked by two lower readings or by interpolation over a short distance between the two highest readings on the trace: and (iii) there is no intersection with another fault and no obvious interference with adjacent faults. Each sample represents half of a complete trace and in some cases two samples are available from a single fault trace. All fault traces are from seam plans in areas where seams dip at less than 15° and so all traces represent horizontal or sub-horizontal chords on the fault planes. Most of the faults have normal throws and are tectonic in origin but some samples may represent compaction faults or synsedimentary faults which cannot

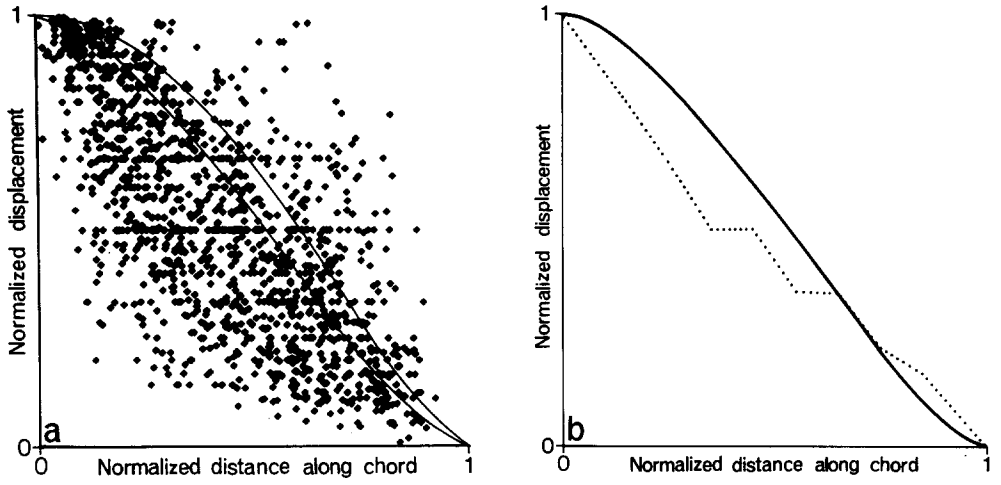

Fig. 5(a). Normalized displacement profile plot for coalfield fault trace data (n = 1354). Theoretical profiles along the radius and along a chord at 0.999 radial distance from the centre of the fault are shown (see Fig. 4). See text for details. (b) Median displacement profile curve for coalfield fault trace data in (a), derived by calculating median normalized displacement values for 10 class intervals along profile. The theoretical displacement profile for a fault radius is shown as the solid curve.

always be distinguished on mine plans. The displacement measurements in all cases are of vertical displacement or throw, and have not been corrected. Fault dips in this coalfield average 68° but dips of the individual faults which the sampled traces represent cannot be determined. The major source of error in the data is believed to be the partial accommodation of displacement by ductile drag rather than by discontinuous slip, where only the latter may be recorded. The extent of this error for any individual fault or displacement reading cannot be determined, but irregular distribution of displacement on some faults is likely to be due to this cause. No attempt has been made to select faults on the basis of the regularity or otherwise of the recorded displacement variation.

The data assembled are from 300 faults giving 488 half-trace samples. Lengths of the half-traces range from 35 to 1300 m and maximum displacements from 10 cm to 13.75 m: the lengths and maximum displacements of the traces do not, of course, necessarily represent those of the actual faults. The number of displacement measurements on individual faults (excluding maximum and zero throws) varies from 1 to 21 with a total of 1354 obtained from all sample traces. All traces have been extended by 50 m before plotting for the reasons outlined previously. These displacement measurements are all included on the normalized diagram shown in Fig. 5(a). Lines of data points at some values of normalized displacement are due to rounding of measurements which, particularly in small faults, produces many measurements which are 0.33, 0.5 or 0.67 of the maximum. The median value profile for 10 class intervals of normalized distance, together with the theoretical profile, are plotted in Fig. 5(b). There is clearly a significant and systematic difference between the data profile and the theoretical profile, with the data in the middle parts of the profile showing displacement values much lower than expected. To examine these differences more closely, the data have been subdivided according to maximum displacements on each trace: traces with maximum throw $\leq$1 m yield 565 displacement measurements; those with maximum throws >1 m and $\geq$2 m yield 499 measurements; and traces with maximum throws >2 m yield 290 measurements (Fig. 6a–c). The composite profiles for the three size groups, each derived from the median values in 10 class intervals, are given in Fig. 6(d) and show systematic differences with the departure from the theoretical profile increasing with fault size.

Differences between the data profiles and the theoretical profile, and the differences between the three data profiles could be due to the following factors.

(i) The theoretical profile may not be a good description of displacement variation on faults. In view of the good fit with data on contoured faults this is thought unlikely.

(ii) Systematic errors in either the recording of fault data or in the selection of the fault traces may be included in the data set: possible sources of such errors have been examined and rejected as likely causes of the discrepancy.

(iii) Ductile drag was regarded at the outset as a likely cause of some inaccuracy in the recorded displacement measurements, but is now considered to be the dominant cause of differences between the size grouped data profiles and between the data and theoretical profiles.

Ductile drag

Under-recording of displacement, by failure to record that accommodated by ductile drag, will not have a significant effect on a displacement profile if the proportion of displacement accommodated by drag is constant along a fault. The displacement profile derived from all data (Fig. 5b) could only show the systematic difference from the theoretical profile if the maximum throw values were either not affected by drag or affected to a lesser

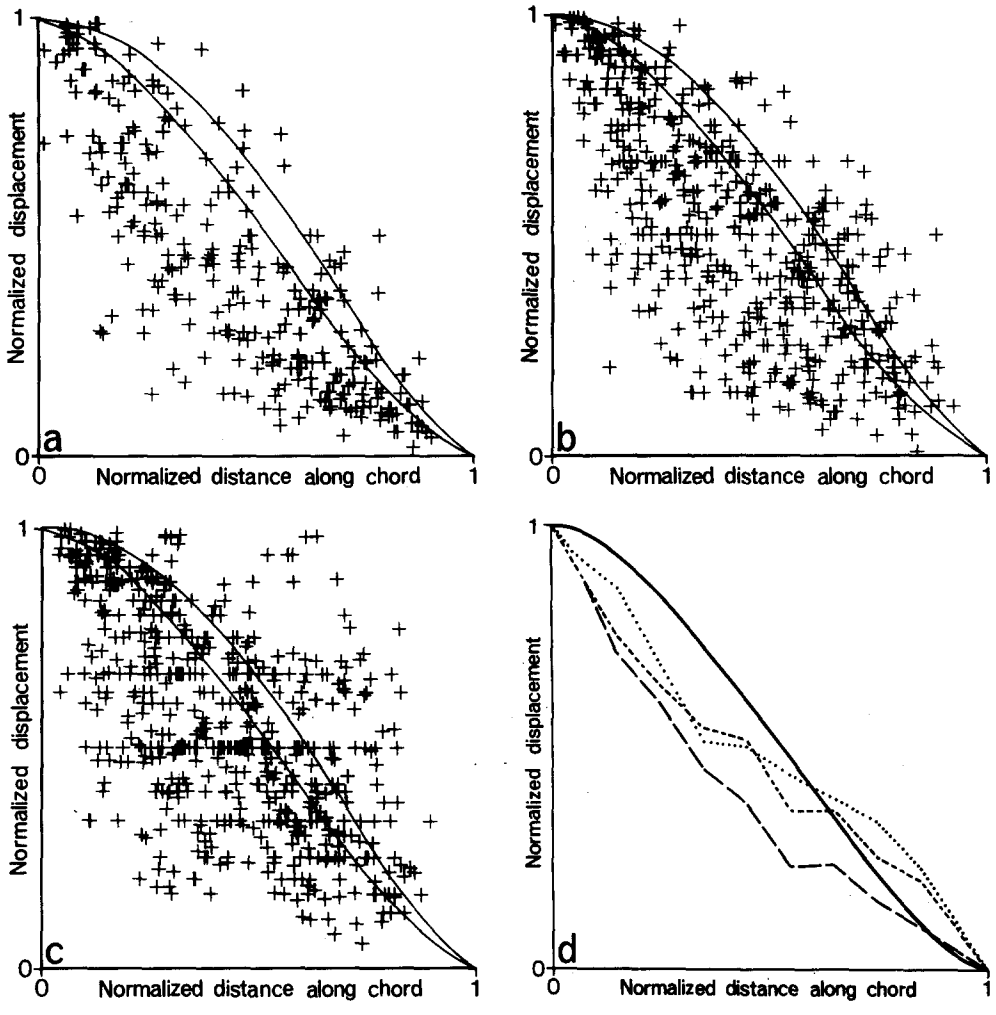

Fig. 6. Normalized displacement profile plots for coalfield fault trace data with maximum displacements of (a) greater than 2 m, (b) greater than 1 m and up to 2 m, and (c) 1 m or less. Theoretical profiles along the radius and along the chord at 0.999 radial distance from the fault centre are also shown. (d) Median curves for each of the normalized displacement profile plots, derived by calculating median normalized displacement value for 10 class intervals along each profile. The highest class interval contains few data points and is therefore ignored; long dashed curve—greater than 2 m maximum displacement, short dashed curve—greater than 1 m and up to 2 m, dotted curve—1 m or less, solid curve—theoretical displacement profile along fault radius.

extent than throw values elsewhere on the fault traces. The size grouped profiles show that with increasing size of the maximum throw measurement, the other throw values depart further, both in absolute and relative terms, from the expected values. Confirmation that the data profiles are the result of consistently low displacement measurements, to varying degrees, is provided by the plot of displacement measurements on faults of maximum throw >2 m (Fig. 6a), which is thought to be the most reliable data set. The theoretical profiles lie along the upper boundary of the concentration of data points: this can also be recognized on the plot of data from faults between 1 and 2 m (Fig. 6b) and even on that for faults ≤1 m (Fig. 6c) although here the data distribution is much less systematic. The conclusion drawn is that although maximum values of displacement are accurately recorded in the data, displacement values elsewhere on fault traces are frequently less than the true values, and that this is due to the frequent failure to record the displacement accommodated by the ductile drag. Where the total displacement, including the drag component, is small enough to be seen on a working face, it is more likely that the drag component is included in the recorded measurement.

Although ductile drag is indicated as being very significant in these faults, the data are in some respects neither representative of faults in general nor even of the faults sampled. Drag is likely to be best developed in the more ductile layers and therefore to affect coal seams more than most other rocks in the succession, and all the data are of measured displacement of coal seams. The distribution of ductile drag on individual faults cannot be investigated from the data available, but many faults have very irregular displacement profiles which would be expected if drag effects varied in an unsystematic way: however, the displacement measurements on a single fault trace may have been made over many years without a consistent policy on whether or not to include the displacement accommodated by drag. Drag effects are minimized in the data from contoured faults for which the composite displacement profile closely matches the theoretical profile. This is mainly because

displacement data on the larger contoured faults are derived from seam contours, rather than from recorded measurements, and this method automatically includes any displacement due to drag. Additionally, a prerequisite for contouring faults with maximum displacement up to 10 m is systematic displacement measurements.

The apparent absence of drag effects on the measurements of maximum displacement on fault traces, could be due to the preferred selection of those traces where the maximum displacement is identifiable because there is no drag. This is thought unlikely, especially for faults larger than 2 m where only a few faults were rejected because the maximum could not be identified. A preferred explanation is that the faults initiated as brittle fractures without a precursory monocline. During subsequent growth of a fault the radially migrating elliptical tip-line is preceded by a monoclinal flexure, the amplitude of the flexure increasing with size of the fault, which when intersected by the propagating fracture is seen as ductile drag. If drag developed, or continued to develop adjacent to, rather than ahead of, the fracture it would be expected to occur also at the maximum displacement. The proposed relationships are well illustrated in the diagram reproduced as Fig. 7 which shows systematic variations in drag adjacent to the fracture with monoclinal flexuring ahead of the propagating lateral tip. The interpretation of the data which we have proposed, requires drag to be absent not only from the central region of the fault surface ellipse, but also from a linear zone extending upwards and downwards from the centre to the tip-line. This is a requirement because the maximum displacements on the analysed fault traces do not represent mid-points of fault surfaces but some point along the down-dip principal axis of the fault surface ellipse. The inferred relationships would occur if monoclinal flexures developed only in response to the lateral component of tip-line propagation: i.e. only in beds in which a fracture had already formed, and not in beds above the top-most part of the tip-line or in those below the bottom-most part of the tip-line.

Ductile deformation in the vicinity of a fault originates in one of three ways: (i) that which is geometrically necessary to accommodate variable displacement (Coward 1976); (ii) that which is geometrically necessary to accommodate slip on a non-planar surface; and (iii) that which is not geometrically necessary but which may occur if certain mechanical conditions obtain. The difference between a discontinuous fault and a ductile shear zone is essentially one of variation of this category of ductile strain. The term "ductile bead" was coined by Elliott (1976) to refer to this category of strain but the useful distinction has not subsequently been maintained (e.g. Coward & Potts 1983, Watterson 1986). The ductile flexuring producing drag on the coalfield faults constitutes a ductile bead as originally defined, and its occurrence depends on appropriate relationships between the work required to create and propagate a fracture and the work required for ductile strain: a low ductile yield stress will favour the formation of a ductile bead (Elliott 1976). However, the work required to initiate and propagate Mode II (edge dislocation) and Mode III (screw dislocation) fractures is not identical and, in the same material, a ductile bead may be associated with one and not with the other. The coalfield data are consistent with ductile flexuring preceding the laterally propagating fault tips (i.e. the Mode III component), but not preceding the upwards and downwards propagating tips (i.e. the Mode II component of the fracture). It is not suggested that this will always be the case, even for coalfield faults: where an incompetent layer is present (e.g. shale), an abrupt upward or downward termination of the fault discontinuity may occur at the incompetent layer, accompanied by folding of an adjacent unfaulted competent layer.

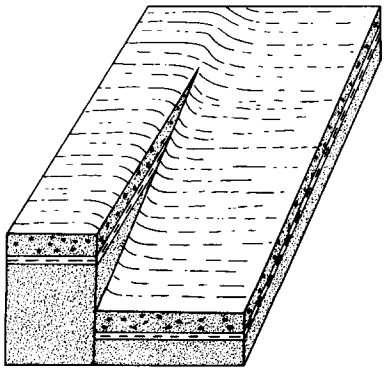

Fig. 7. Schematic diagram of a fault showing varying degrees of ductile drag adjacent to the fracture and associated monoclinal flexuring ahead of the propagating lateral tip. (Redrawn from Chamberlin and Salisbury, in Geikie 1912.)

CONCLUSION

Interpretation of the seismic spectra of earthquake events requires assumptions to be made regarding both the shape of the slipped surface and the distribution of the slip over this surface. In general, direct observation can be made only on inactive faults and such observations provide information only on the final shape and distribution of displacement on the fault surface, both of which are the product of a large number of single slip events or a long period of stable sliding. Given some basic assumptions regarding fault growth, it is possible to determine whether or not a particular pattern of incremental slip is compatible with a particular pattern of finite displacement. The composite displacement profile of faults in English coalfields has been shown to be compatible with the Eshelby model for slip distribution during a single slip event. Further investigations of inactive faults, particularly with regard to mean displacement gradients, to displacement profiles and to the elastic and mechanical properties of the rocks concerned, can be expected to provide useful constraints on the static characteristics of single slip events. For these purposes it is important that the elastic and mechanical properties of the faulted rocks should not have changed significantly since the faulting took place and a good

knowledge of the geological history of the faulted rocks is required.

Acknowledgements—The authors thank John Rippon and Jim Barnett for access to contoured fault data and John Mortimer and Iwan Williams for assistance with collection and analysis of mine plans. The Liverpool Fault Analysis Group is funded by NERC (grant GR3/4719), British Coal (contract YCE.30/19572) and the USGS Earthquake Hazards Reduction Program (contract 14-08-0001-22072). This paper is published with the permission of British Coal but the opinions expressed are the authors and do not necessarily represent those of British Coal.

REFERENCES

Archuleta, R. J. & Brune, J. N. 1975. Surface strong motion associated with a stick–slip event in a foam rubber model of earthquakes. *Bull. seism. Soc. Am.* **65**, 1059–1071.

Barnett, J., Mortimer, J., Rippon, J., Walsh, J. J. & Watterson, J. 1987. Displacement geometry in the volume containing a single normal fault. *Am. Ass. Petrol. Geol.* In press.

Coward, M. P. 1976. Strain within ductile shear zones. *Tectonophysics* **34**, 181–197.

Coward, M. P. & Potts, G. J. 1983. Complex strain patterns at the frontal and lateral tips to shear zones and thrust zones. *J. Struct. Geol.* **5**, 383–399.

Elliott, D. 1976. The energy balance and deformation mechanisms of thrust sheets. *Phil. Trans. R. Soc. Lond.* **A283**, 289–312.

Eshelby, J. D. 1957. The determination of the elastic field of an ellipsoidal inclusion and related problems. *Phil. Trans R. Soc. Lond.* **A241**, 376–396.

Geikie, A. 1912. *Structural and Field Geology*. Oliver and Boyd, Edinburgh.

Kanamori, H. & Anderson, D. L. 1975. Theoretical basis of some empirical relations in seismology. *Bull. seism. Soc. Am.* **65**, 1075–1095.

Muraoka, H. & Kamata, H. 1983. Displacement distribution along minor fault traces. *J. Struct. Geol.* **5**, 483–495.

Rippon, J. 1985. Contoured patterns of the throw and hade of normal faults in the Coal Measures (Westphalian) of north-east Derbyshire. *Proc. Yorks. geol. Soc.* **45**, 147–161.

Scholz, C. H. 1982. Scaling laws for large earthquakes: consequences for physical models. *Bull. seism. Soc. Am.* **72**, 1–14.

Walsh, J. J. & Watterson, J. 1987. Analysis of the relationship between displacements and dimensions of faults. *J. Struct. Geol.* In review.

Watterson, J. 1986. Fault dimensions, displacements and growth. *Pure appl. Geophys.* **124**, 365–373.

APPENDIX

The normalized slip distribution on a fault plane for a series of successive slip events is represented by the circles r_1 to r_n, concentric about the centre, C, of the fault (Fig. A1). The final fault radius, R, is also the radius of the final slip event. The maximum slip in the final slip event, U, is at C and is a linear function of R.

The cumulative slip (displacement), D, at C is the sum of n slip events in which the successive slips, $U_1 + U_2 \ldots U_n$, form an arithmetic series with common difference a and first term zero.

$$D = n/2(n-1)a$$

but when n is large, $D = n^2a/2$.

As $U = a \times n$,

$$D = (U^2 \times a)/2a^2$$

so

$$D = U^2/2a.$$

The displacement, d, at a point, l, at radial distance l from the centre of the fault, is the sum of all the slip events at this point

$$d = S\{u_1 + u_2 + \ldots + u_n\}.$$

The values of u_1, u_2, etc., are given by the intersections along the perpendicular from L with the circles representing the slip in each separate event. The mean value of these slips, u_m, is given by the intersection on the perpendicular from L with the circle of radius midway between the radii of the first and last slip events to have contributed to slip at L, i.e. a circle of radius $= (R + r)/2$ (see below).

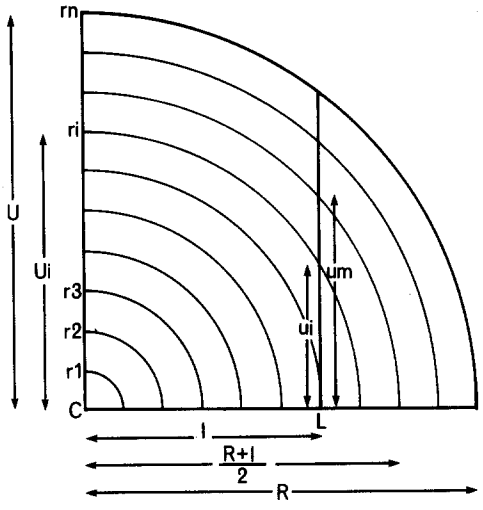

Fig. A1. Normalized slip (ordinate) vs normalized radial distance from fault centre (abscissa). See text for details.

The mean slip at L is given by

$$u_m = (((R + r)/2)^2 - l^2)^{1/2}.$$

The number of slips, n_L, which contribute to the mean is given by

$$n_L = n((R - l)/R).$$

The total slip at L, u_L, is therefore

$$u_L = (((R + l)/2)^2 - l^2)^{1/2}((R - l)/R)n$$

when D and R are normalized to 1 this reduces to

$$y = (((1 + x)/2)^2 - x^2)^{1/2}2(1 - x),$$

where y = normalized displacement
x = normalized radial distance from the centre.

It can be demonstrated that the value of u_m can be obtained in the manner shown by reference to Fig. A2. A slip event, i, gives rise to slip u_i at point L on the fault radius where

$$u_i = l \times \tan [\theta]_i,$$

where $[\theta]_i = \cos^{-1}(l/U_i)$.

The mean value of $[\theta]$, $[\theta]_m$, for all slips at L is

$$[\theta]_m = \cos^{-1}(l/\text{mean radius}) = \cos^{-1}(l/((R + l)/2)).$$

That is, the value of the mean slip at L is given by the intersection of the perpendicular from L with the circle of radius $= (R + l)/2$.

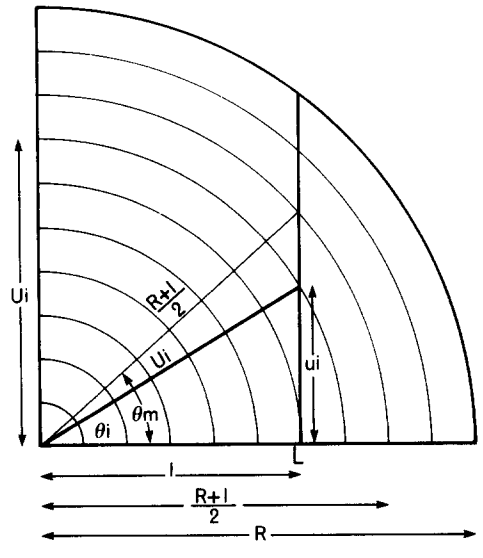

Fig. A2. Normalized slip (ordinate) vs normalized distance from fault centre (abscissa). See text for details.